Electronic Supplementary Material (ESI) for Dalton Transactions.

Supporting Information

Doping Transition Metals to Modulate the Chirality and Photocatalytic Activity of Rare Earth Clusters

Ying Lu, Wen-Zhu Yang, Xiu-Xia Ding, Si-Qi Nie, Zhan-Guo Jiang*, Cai-Hong Zhan*

Key Laboratory of the Ministry of Education for Advanced Catalysis Material
Institute of Physical Chemistry, College of Chemistry and Materials Science
Zhejiang Normal University
Jinhua 321004, P.R. China
E-mail: jzg@zjnu.cn; chzhan@zjnu.cn

Chemicals.

In the synthesis process of the used analytically pure are all the commercial sources and were received without further purification.

Physical Characterizations

Photocatalytic reduction of CO_2 was performed in a 250 mL quartz reactor with as-prepared crystal. Photocatalyst (15 mg) was added into the mixed solution which contained H_2O (45 mL), photosensitizer ($Ru(bppy)_3$, 5 mg) and triethanolamine (TEOA, 5mL) as an electron donor. After degassing with high-purity CO_2 to remove dissolved O_2 for 30 min. Light source is the xenon (Xe) lamp (300 W, CEL-HXF300-T，CHINA EDUCATION AU-LIGHT, China). The reaction temperature was controlled at 303K by using the cooling water circulation. The gas products analyzed by gas chromatograph (FULIGC9790II gas chromatograph, China) with flame ionization detector.

Powder XRD patterns were obtained using a Bruker D8 Advance X-ray diffractometer with (λ (CuKα) = 1.5405 Å) radiation. The materials were recorded on KBr disk using a Nicolet NEXUS 670 spectrometer between 400 and 4000 cm^{-1} in situ FT-IR Spectrometer. C H N microanalyses were performed on a Perkin-Elmer 240C elemental analyzer. The compounds **1-4** were carried out on a TA Instruments STA499 F5 thermobalance with a 100 $mL \cdot min^{-1}$ flow of nitrogen; the temperature was ramped from 20 °C to 800 °C at a rate of 10 $°C \cdot min^{-1}$. A suitable crystal of **1-4** were mounted in a Hampton cryoloop with Paratone® N oil cryoprotectant. Intensity data collections were carried out with a Bruker D8 VENTURE diffractometer equipped with a PHOTON 100 CMOS bidimensional detector using a high brilliance IμS microfocus X-ray Mo/Cu Ka monochromatized radiation. With the aid of Olex2, the structure was solved with the ShelXT structure solution program using Intrinsic Phasing and refined with the ShelXL refinement package using Least Squares minimization.[1] The Solvent-Mask (= SQUEEZE) was employed in the structural refinements to remove the undefined solvents. SIMU has been used to model rational structures. The hydrogen atoms of organic ligands were generated geometrically, H of μ_3-O does was not generated and included in the molecular formula in CIF. Further details about of the crystal structure determinations may be obtained free of charge via the Internet at https://www.ccdc.cam.ac.uk/ CCDC 2277059, 2277122, 2277123 and 2277124. The B level alerts of **2-4** have been responded in the checkCIF files.

Synthesis

Compound **1**: $La_6Mn(\mu_3\text{-}OH)_8(acac)_{12}(CH_3OH)_8$ {La_6Mn}

$La(NO_3)_3\cdot 6H_2O$ (1.00 mmol, 353.4 mg) was dissolved in 1.5 mL of MeOH and added Hacac (2.00 mmol, 205 μL) into the solution. Then, $MnCl_2\cdot 4H_2O$ (0.1 mmol, 19.8 mg) was dissolved in 1.5 mL of MeOH and Et_3N (4.00 mmol, 550 μL) were successively added dropwise into the above solution. The mixture was sealed in a 10 mL vial and shook to make it homogeneous. Compound **1** was obtained after 1 day in a low-temperature environment of 2-6 ℃ (35.6% yield based on $La(NO_3)_3\cdot 6H_2O$). Anal. Calcd for $C_{68}H_{124}O_{40}La_6Mn$ (FW= 2470.26): C, 33.06; H, 5.72; O, 25.91 (%); Found: C, 33.18; H, 5.14; O, 28.22 (%). IR-ATR (cm^{-1}): 1596(s), 1515(vs), 1450 (s), 1381vs), 1255(s), 1194(w), 1014(m), 919(m), 759 (m), 654 (m) 528 (s).

Compound **2**: $La_6Co(\mu_3\text{-}OH)_8(acac)_{12}(CH_3O)_4CH_3OH)_4$ {La_6Co}

$La(NO_3)_3\cdot 6H_2O$ (1.00 mmol, 353.4 mg) wase dissolved in 1.5 mL of MeOH and added Hacac (2.00 mmol, 205 μL) into the solution. Then, $Co(NO_3)_3\cdot 6H_2O$ (0.1 mmol, 29.1 mg) was dissolved in 1.5 mL of MeOH and Et_3N (4.00 mmol, 550 μL) were successively added dropwise into the above solution. The mixture was sealed in a 10 mL vial and shook to make it homogeneous. Compound **2** was obtained after 3 days in a low-temperature environment of 2-6 ℃ (35.6% yield based on $La(NO_3)_3\cdot 6H_2O$). Anal. Calcd for $C_{68}H_{120}O_{40}La_6Co$ (FW= 2470.21): C, 33.06; H, 4.91; O, 25.91 (%); Found: C, 33.16; H, 5.04; O, 29.02 (%). IR-ATR (cm^{-1}): 1596 (s), 1513 (vs), 1450 (s), 1386 (vs), 1255 (s), 1197 (w), 1018 (m), 918 (m), 759 (m),655 (m), 524 (s).

Compound **3**: $La_6Fe(\mu_3\text{-}OH)_8(acac)_{12}(CH_3O)_4CH_3OH)_4$ {La_6Fe}

$La(NO_3)_3\cdot 6H_2O$ (1.00 mmol, 353.4 mg) was dissolved in 1.5 mL of MeOH and added Hacac (2.00 mmol, 205 μL) into the solution. Then, $Fe(NO_3)_3\cdot 9H_2O$ (0.1 mmol, 40 mg) was dissolved in 1.5 mL of MeOH and Et_3N (4.00 mmol, 550 μL) were successively added dropwise into the above solution. The mixture was sealed in a 10 mL vial and shook to make it homogeneous. Compound **3** was obtained after 1 day in a low-temperature environment of 2-6 ℃ (33.6% yield based on $La(NO_3)_3\cdot 6H_2O$). Anal. Calcd for $C_{68}H_{120}O_{40}La_6Fe$ (FW= 2467.13): C, 33.12; H, 4.91; O, 25.94 (%); Found: C, 33.54; H, 5.01; O, 28.12 (%). IR-ATR (cm^{-1}): 1598 (s), 1513 (vs), 1452 (s), 1383 (vs), 1253 (s), 1193 (w), 1014 (m), 918 (m), 765 (m),653 (m), 528 (s).

Compound **4**: $Nd_9Fe_2(\mu_4\text{-}O)(\mu_3\text{-}OH)_{14}(acac)_{16}(NO_3)(CH_3OH)_2(H_2O)_3$ {Nd_9Fe_2}

$NdCl_3\cdot 6H_2O$ (1.00 mmol, 353.4 mg) was dissolved in 1.5 mL of MeOH and added Hacac (2.00 mmol, 205 μL) into the solution. Then, $Fe(NO_3)_3\cdot 9H_2O$ (0.3 mmol, 120 mg) was solved in 1.5 mL of MeOH and Et_3N (4.00 mmol, 550 μL) were successively added dropwise into the above solution. The mixture was sealed in a 10 mL vial and shook to make it homogeneous. Compound **4** was obtained after 3 days in a low-temperature environment of 2-6 ℃ (34.6% yield based on $NdCl_3\cdot 6H_2O$). Anal. Calcd for $C_{82}H_{140}NO_{57}Nd_9Fe_2$ (FW= 3459.5): C, 28.44; H, 4.05; O, 26.36 (%); Found: C, 29.18; H, 4.14; O, 26.52 (%). IR-ATR (cm^{-1}): 1599 (s), 1519 (vs), 1454 (s), 1378 (vs), 1259 (s), 1191 (w), 1019 (m), 918 (m), 758 (m), 654 (m), 523 (s).

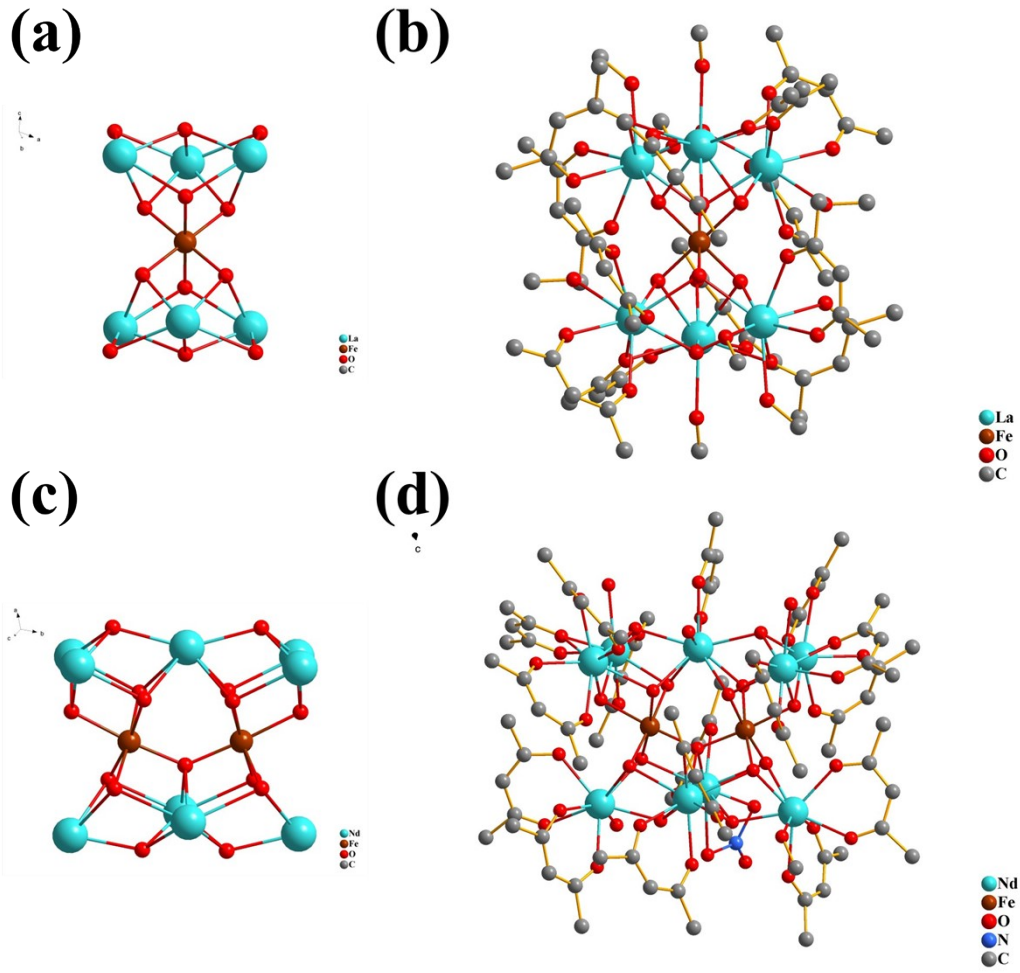

Figure S1. (a) Ball-and-stick view of the combination of two $\{La_3Fe\}$ subunits into the core unit of $\{La_6Fe\}$. (b) Crystal structure of $\{La_6Fe\}$. (c) Ball-and-stick view of the combination of four $\{Nd_3Fe\}$ subunits into the core unit of $\{Nd_9Fe_2\}$. (d) Crystal structure of $\{Nd_9Fe_2\}$. Hydrogen atoms have been omitted for the sake of clarity.

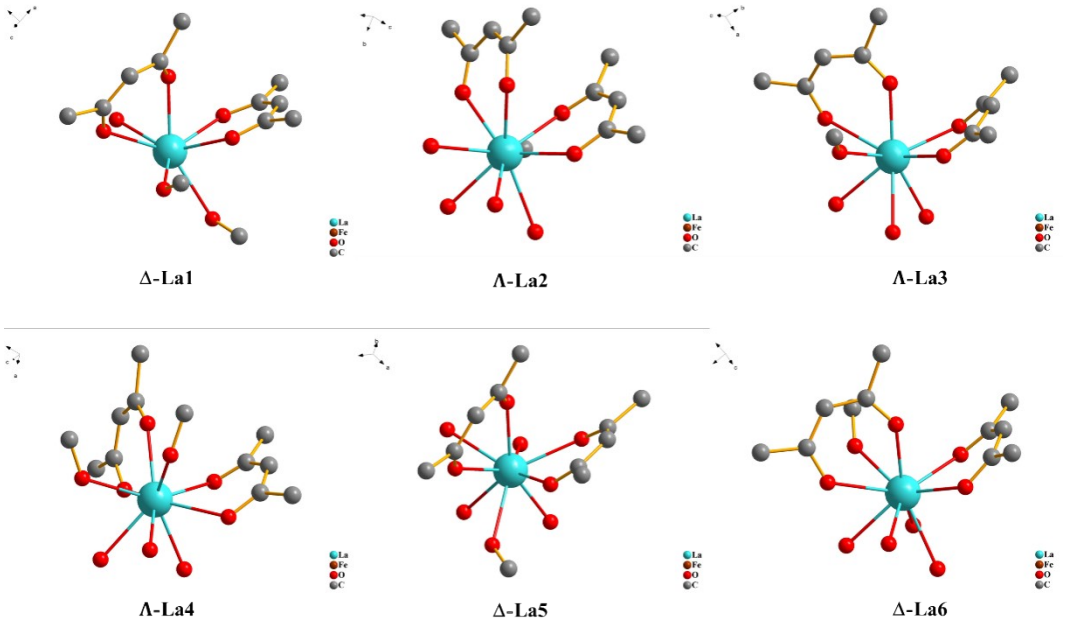

Figure S2. The acac$^-$ coordinates with La^{3+} ion in ΛΛΔΔΔΔ-{La_6Fe}.

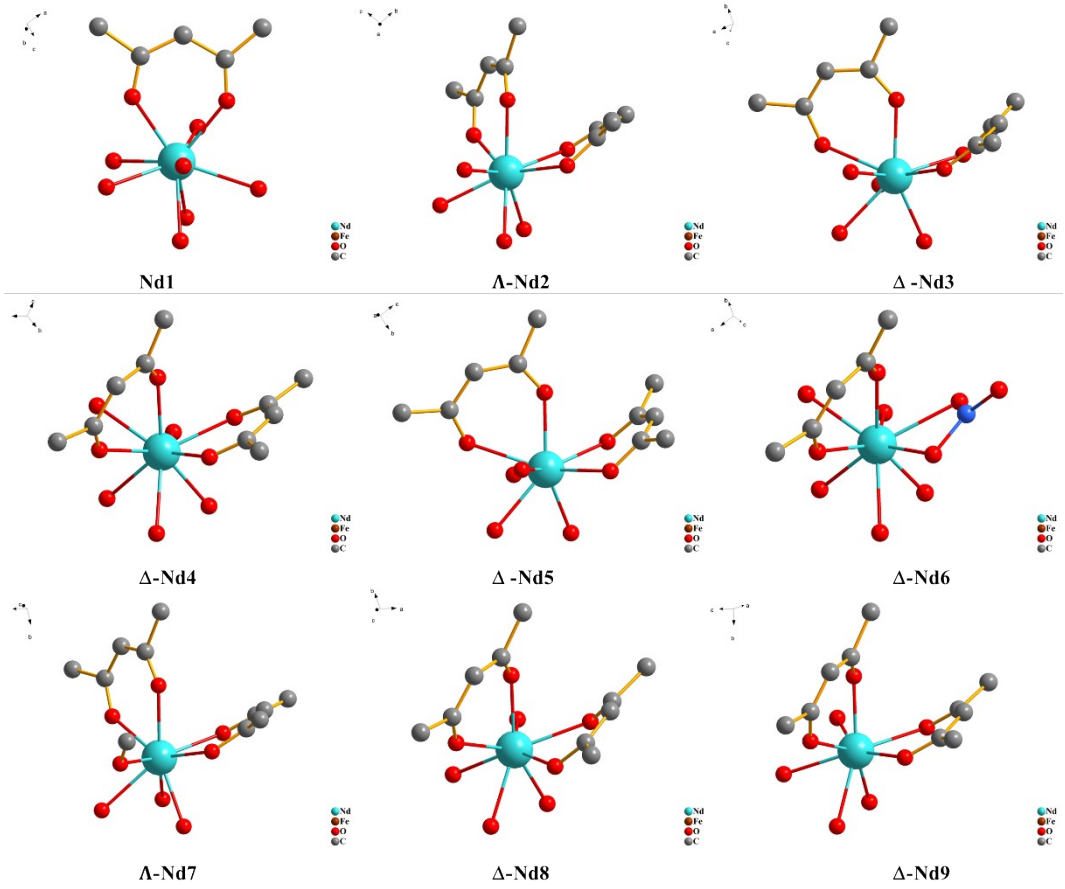

Figure S3. The acac$^-$ coordinates with Nd^{3+} ion in ΔΔΔΔΔΔΛΛ-{Nd_9Fe_2}.

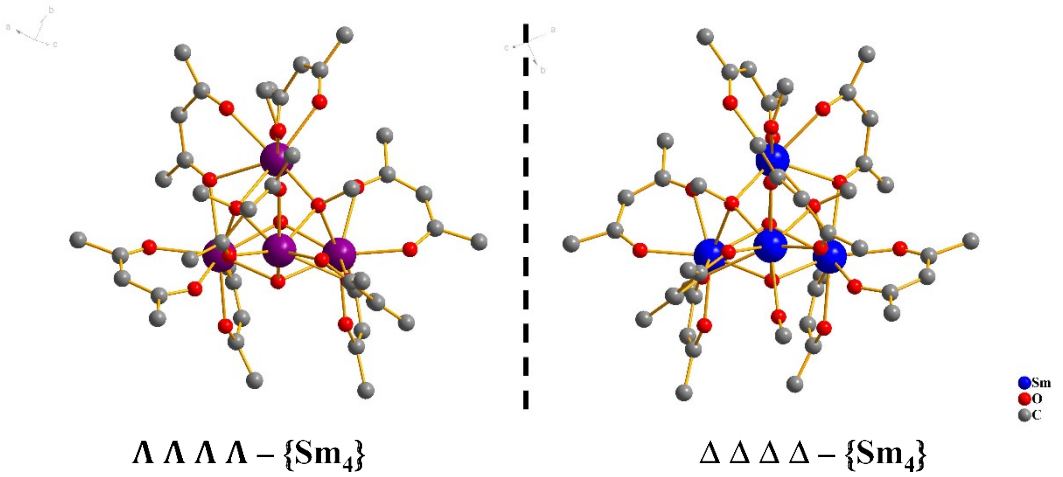

Figure S4. Crystal structure of $\{Sm_4\}$.

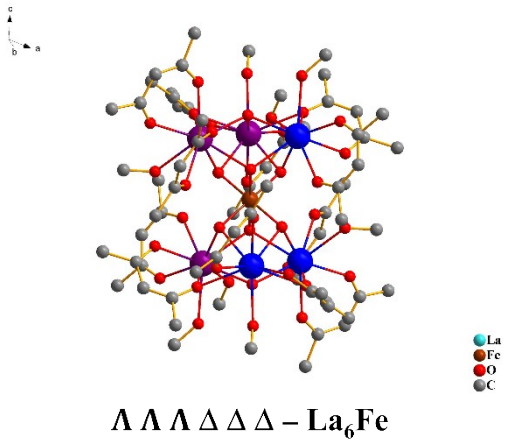

Figure S5. Crystal structure of $\{La_6Fe\}$.

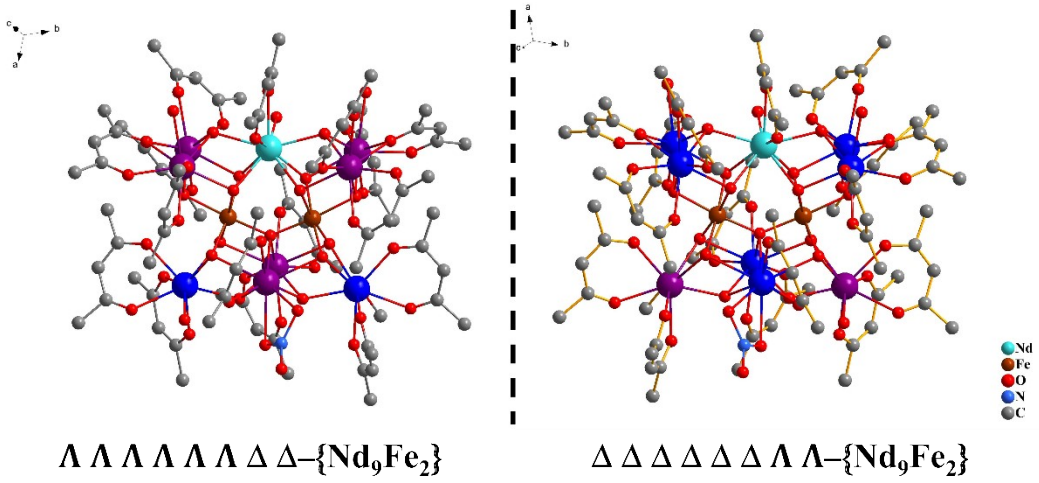

Figure S6. Crystal structure of $\{Nd_9Fe_2\}$.

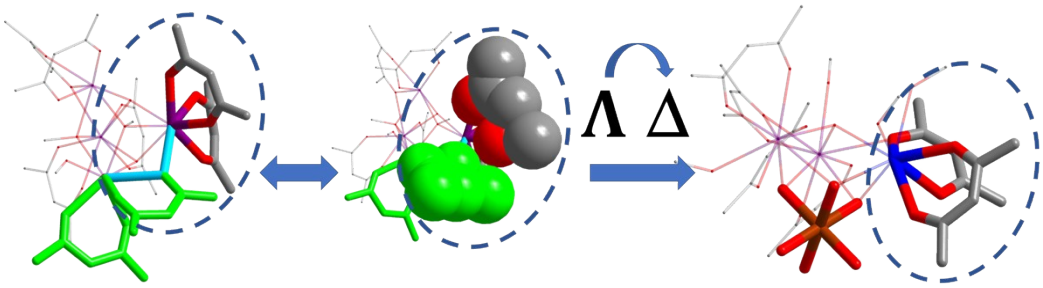

Figure S7. The coordination pattern of La before and after transition metal substitution of {La_3Fe} module.

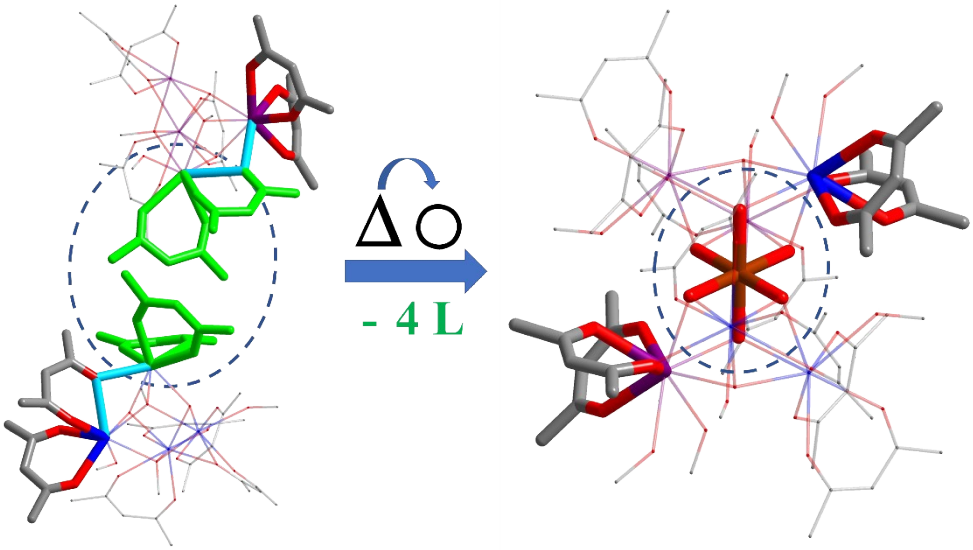

Figure S8. The coordination pattern of La before and after transition metal substitution of {La_6Fe}.

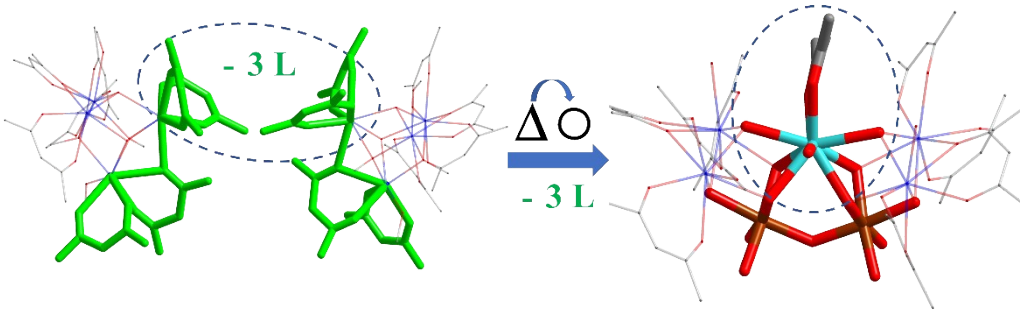

Figure S9. The coordination pattern of Nd before and after transition metal substitution of {Nd_5Fe_2} module.

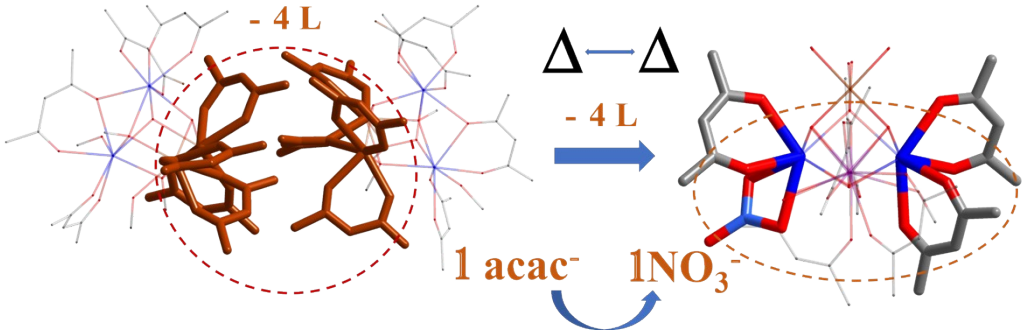

Figure S10. The coordination pattern of Nd before and after transition metal substitution of $\{Nd_4Fe_2\}$ module.

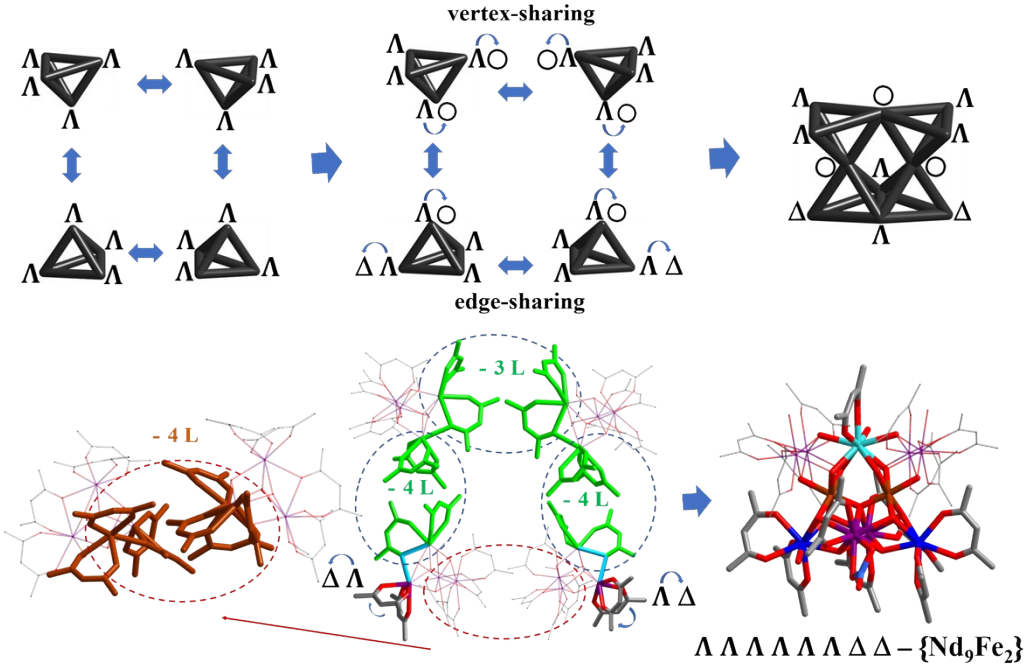

Figure S11. Topological stereochemistry and image of wireframe of ΛΛΛΛΛΛΔΔ–$\{Nd_9Fe_2\}$.

Figure S12. The PXRD of **1**-**4**.

To determine the purity and stability of **1**-**4**, the powder samples of **1**-**4** were tested by powder X-ray diffraction and compared with the spectra obtained by fitting single crystal data. The diffraction peaks of **1**-**4** powder samples are in good agreement with the simulated diffraction peaks, and the intensity values of some diffraction peaks are different, which may be related to the loss of solvent molecules and the size of sample particles. It shows that the sample of **1**-**4** is pure phase and stable at room temperature.

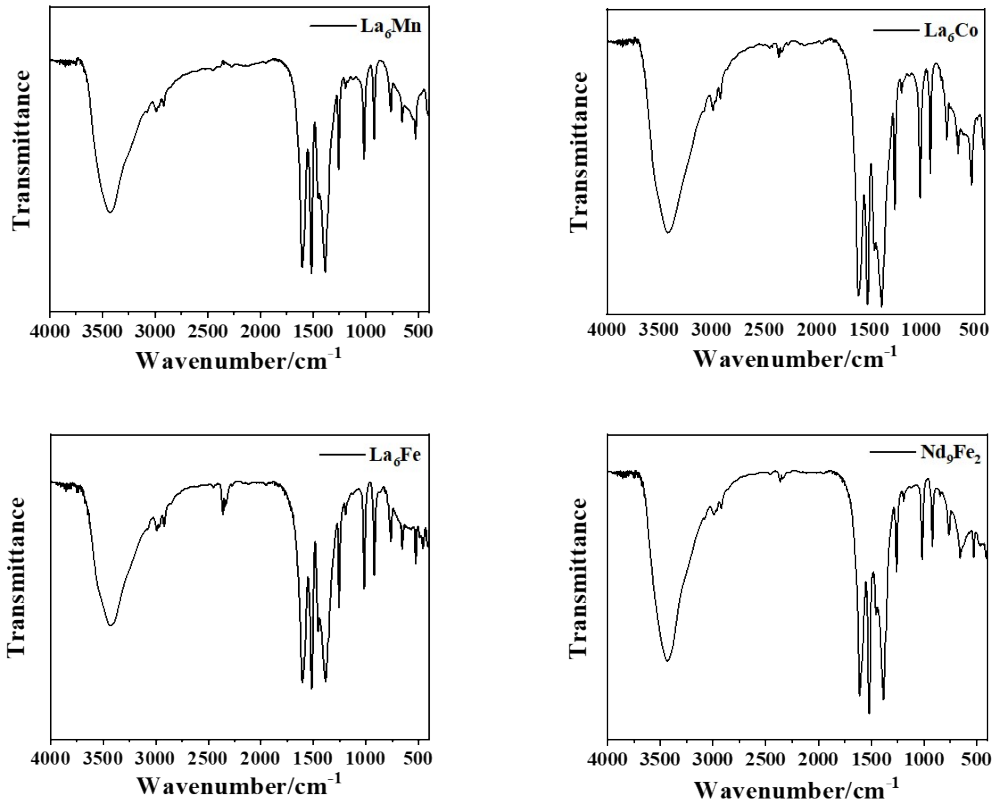

Figure S13. The FT-IR of **1**-**4**.

The broad peak around 2800 cm^{-1} is attributed to the stretching vibration of the O-H. The strong absorption bands from 1630 cm^{-1} to 1060 cm^{-1} were caused by the C=O, C-O and C-C stretching vibration of acetylacetone. The bands from 1060 cm^{-1} to 400 cm^{-1} are mainly attributed to the metal-oxygen vibration.

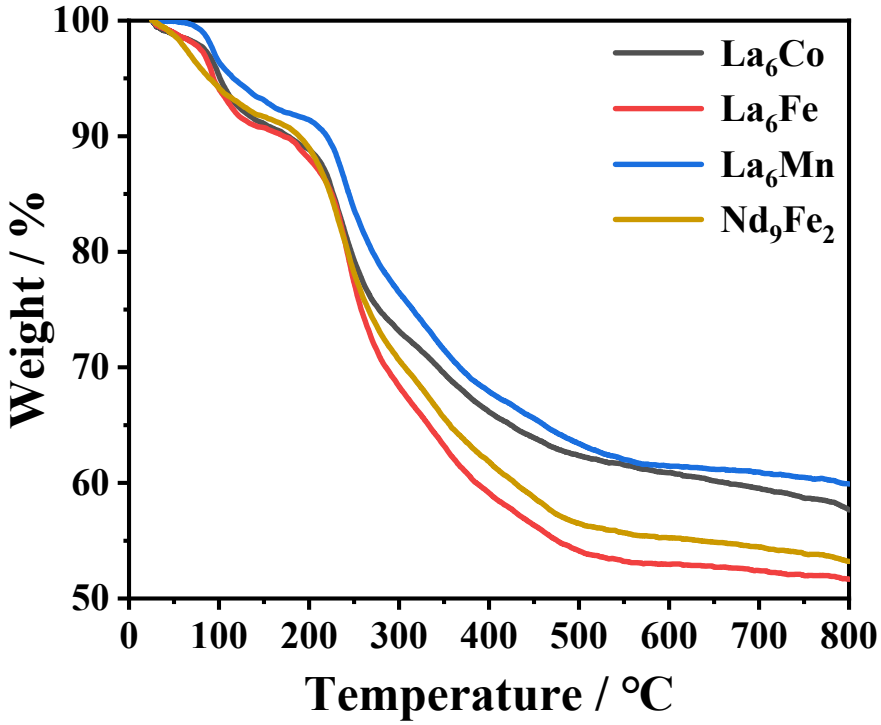

Figure S14. The TGA curve of **1-4** under N_2 atmosphere.

The TGA measurements of **1-4** were under the N_2 atmosphere. The **1-4** display the weight loss of 2.52%, 2.61%, 0.92% and 6.36%, respectively, in the range of rt-100 ℃, which belongs to the departure of the solvent molecules, indicating that the cluster has good thermal stability before 100 ℃. The curves decrease slowly between 100 ℃ and 220 ℃, and it is attributed to the loss of monodentate coordination methanol according to the weight loss rate. As the temperature increases, the frameworks begin to collapse. When the temperature is higher than 220 ℃, the proportion of residual oxides can be calculated to 57.80%, 53.44%, 61.29%, and 62.19%, respectively, in the final.

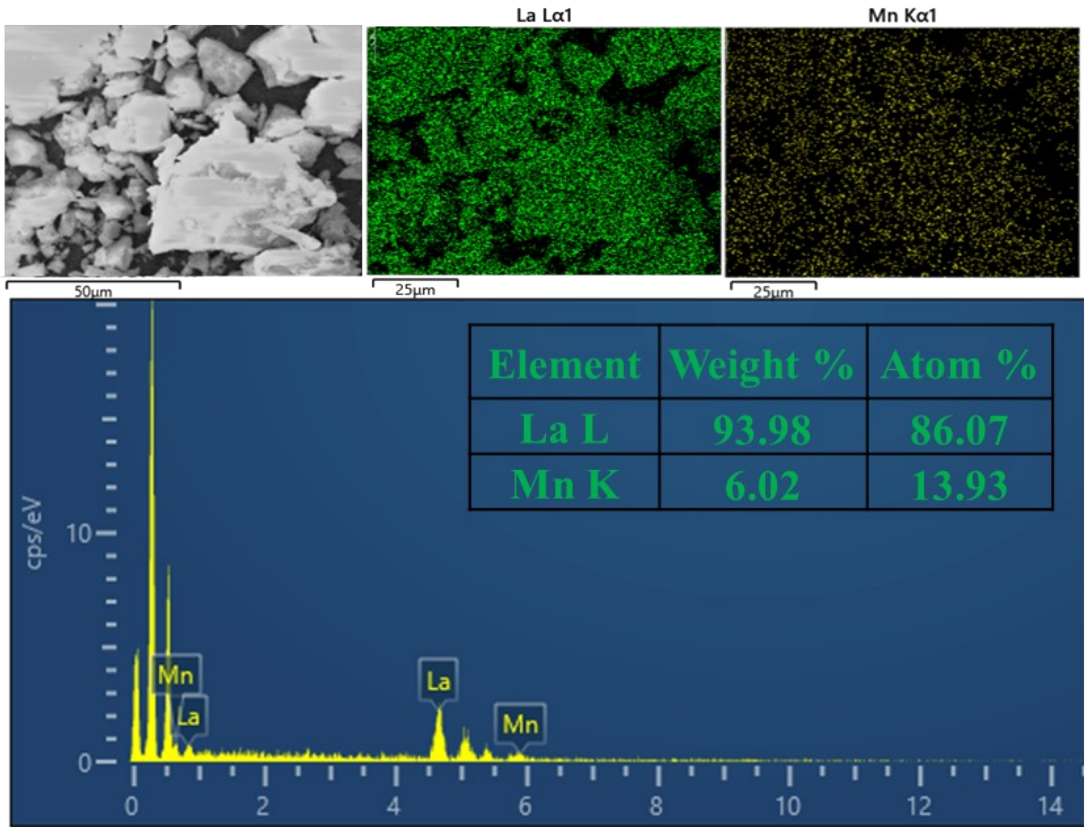

Figure S15. Energy-dispersive X-ray spectroscopy of compound **1**.

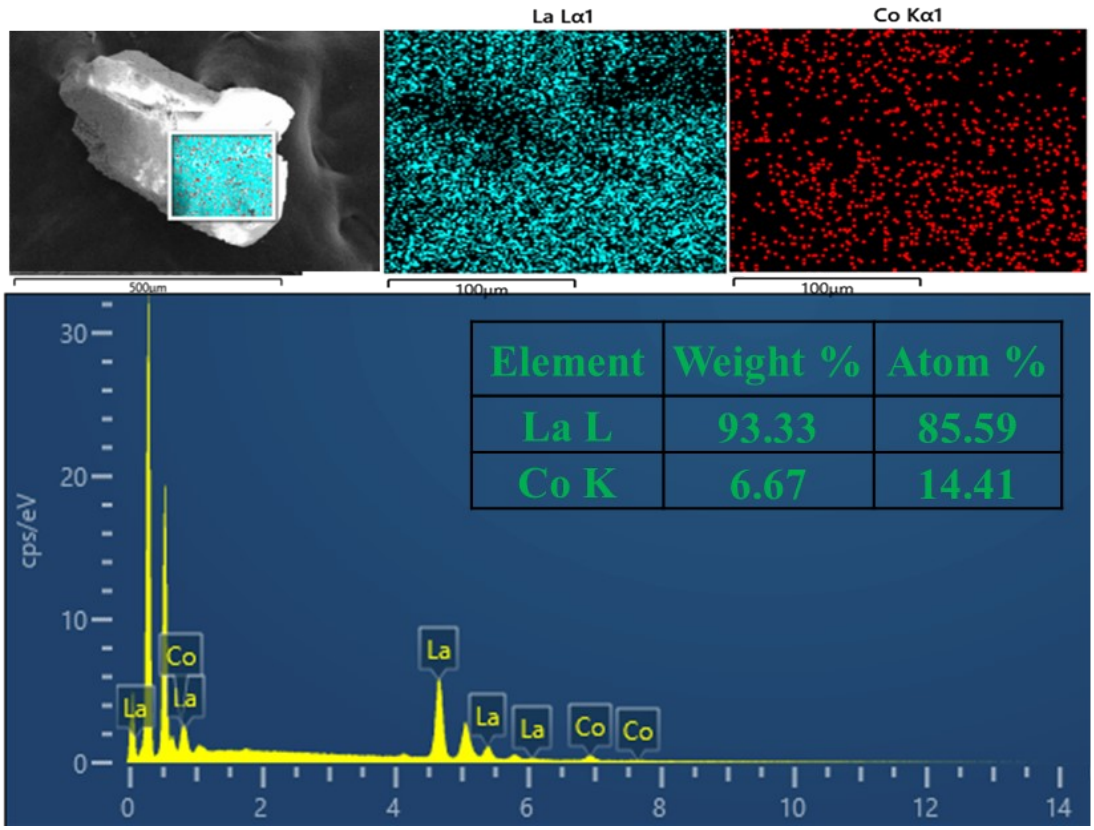

Figure S16. Energy-dispersive X-ray spectroscopy of compound **2**.

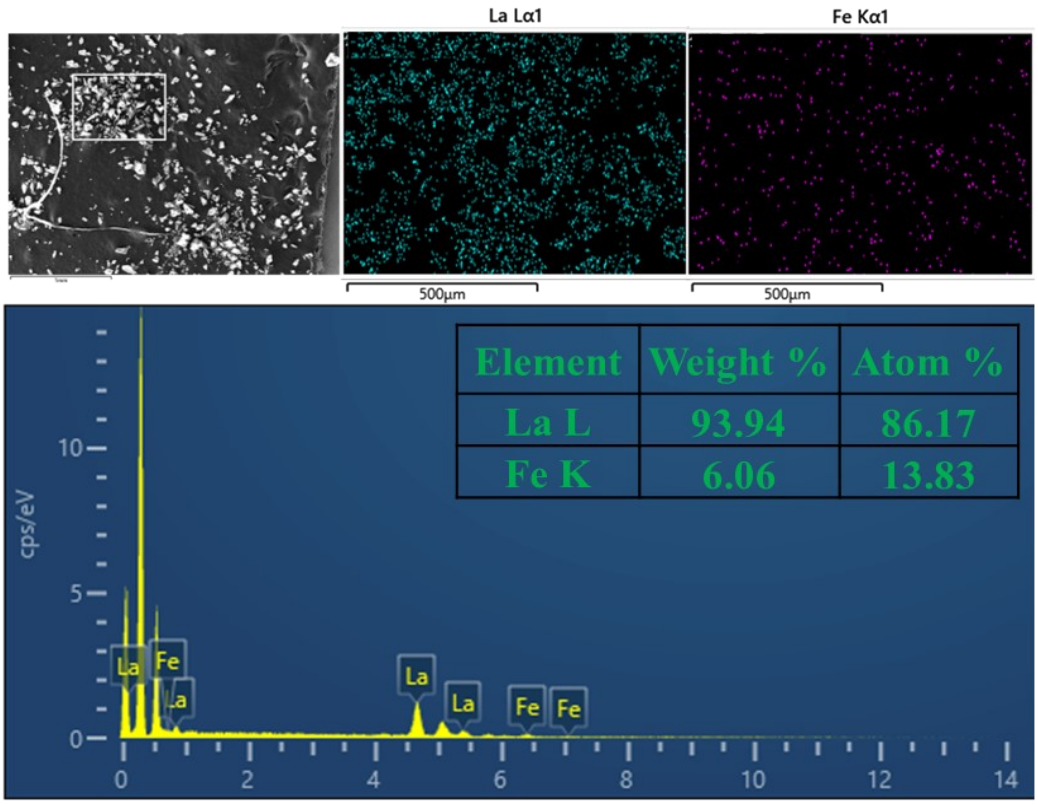

Figure S17. Energy-dispersive X-ray spectroscopy of compound **3**.

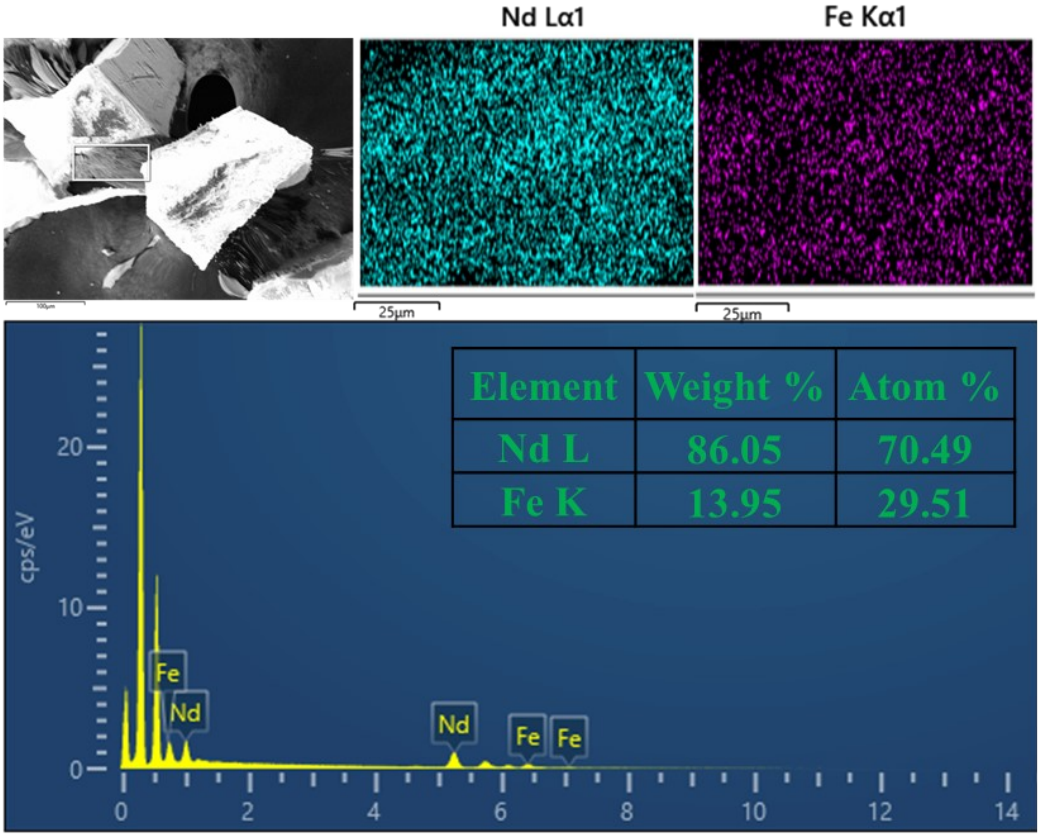

Figure S18. Energy-dispersive X-ray spectroscopy of compound **4**.

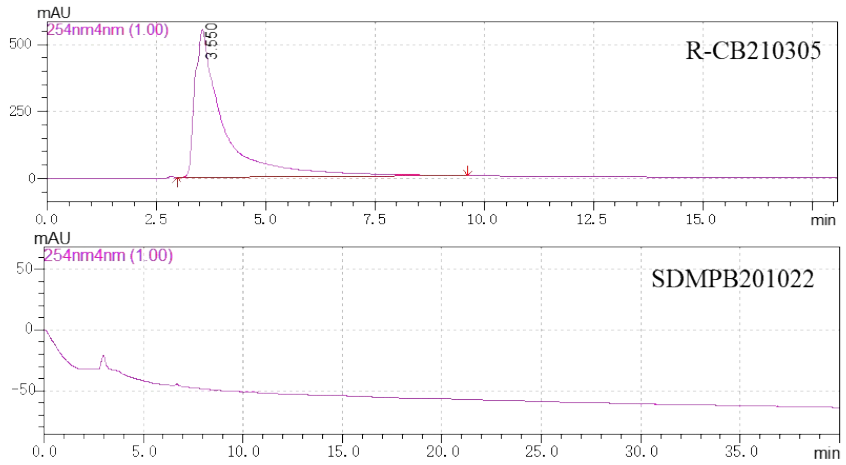

Figure S19. HPLC chromatogram of enantioseparation of racemic $\{Nd_9Fe_2\}$ with chiral liquid chromatography, such as Chiralcel OD-H column (5 μm, 4.6 mm × 250 mm) and Chiralcel IC column (5 μm, 4.6 mm × 250 mm).

Racemic $\{Nd_9Fe_2\}$ was tired to be separated by HPLC on JC-002 system with the UV-Vis detector at 254 nm. The mobile phase was methanol. And the flow rate was 1.0 ml/min. Unfortunately, there is only one peak discerned in whole HPLC chromatogram, indicating that the racemic $\{Nd_9Fe_2\}$ could not be separated by this method.

Attempts of enantiomeric separation of $\{Nd_9Fe_2\}$ are:

(1) Growing single asymmetric crystals (Spontaneous Resolution): Diffusion crystallization; Changing the concentration and speed of solution volatilization; Recrystallization;

(2) Forming diastereoisomers with optically active cations (Diastereomeric crystallization): (R)-(+)- and (S)-(-)-1-Phenylethylamine; (S)-(+)- and (R)-(-)-2-Phenylglycinol; D-$Co(en)_3^{3+}$; (1S,2S)-(+)-and (1R,2R)-(-)-1,2-DiaMinocyclohexane);

(3) Adding a variety of chiral components during synthesis process: amino acid; D- and L-Tartaric acid; trans- and cis-4-Aminocyclohexanecarboxylic acid; trans- and cis-Tranexamic Acid; trans- and cis-1,4-Cyclohexanedicarboxybic acid; (R)-(+)- and (S)-(-)-2,2'-Diamino-1,1'-binaphthalene; (+)- and (-)-1,1'-Bi-2-naphtho;

(4) chiral liquid chromatography.

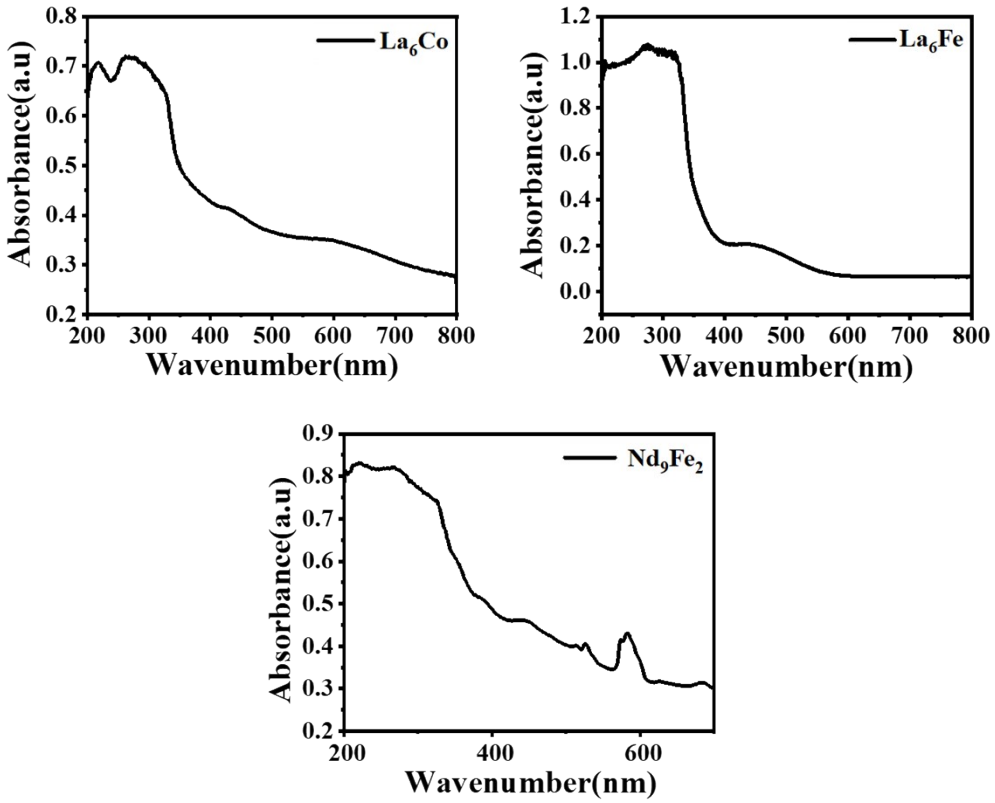

Figure S20. The solid UV-vis of **2**-**4**.

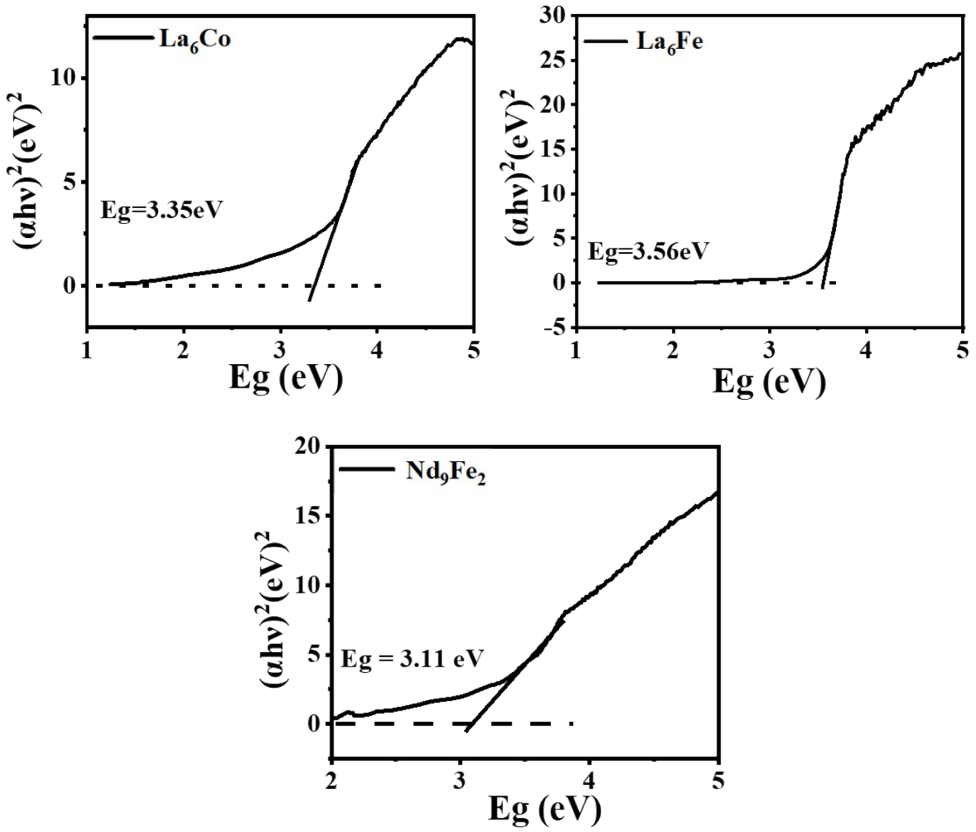

Figure S21. The Band gap energy (Eg) analysis of **2**-**4**.

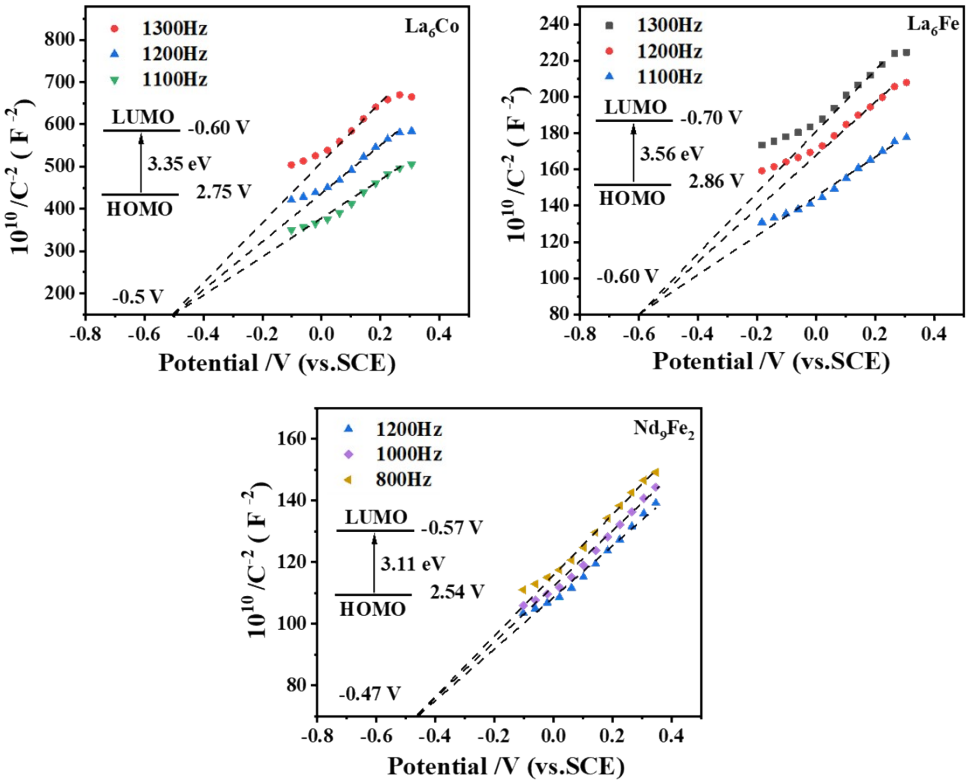

Figure S22. The Mott–Schottky plots for **2-4** in 0.5 M Na_2SO_4 aqueous solution. Inset: The energy diagram of the HOMO and LUMO levels of compounds **2-4**.

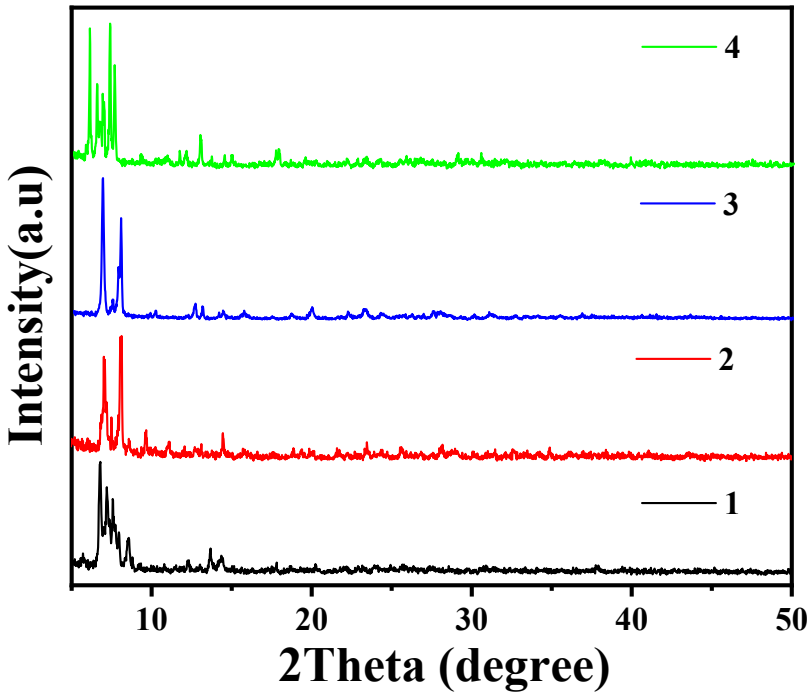

Figure S23. The PXRD of **1-4** after 10 hours in water solution.

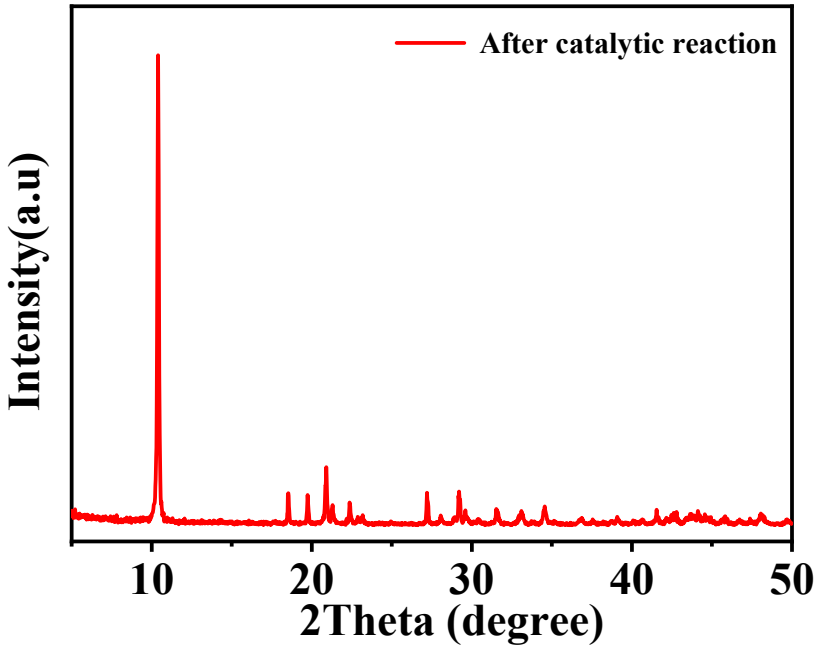

Figure S24. The PXRD of **1** after catalytic reaction.

Table of crystal data.

Identification code	**1**	**2**
Empirical formula	$C_{68}H_{116}La_6MnO_{40}$	$C_{68}H_{112}CoLa_6O_{40}$
Formula weight	2462.00	2461.96
Temperature/K	150.00	298.00
Crystal system	triclinic	monoclinic
Space group	*P*-1	$P2_1/n$
a/Å	14.8299(12)	14.053(5)
b/Å	16.9780(13)	25.317(9)
c/Å	20.0319(16)	14.775(5)
α/°	83.811(3)	90
β/°	85.464(3)	111.095(11)
γ/°	88.201(3)	90
Volume/Å^3	4997.2(7)	4904(3)
Z	2	2
ρ_{calc}g/cm^3	1.636	1.667
μ/mm^{-1}	2.704	2.796
F(000)	2422.0	2418.0
Crystal size/mm^3	0.11 × 0.1 × 0.08	0.11 × 0.1 × 0.09
Radiation	MoKα (λ = 0.71073)	MoKα (λ = 0.71073)
2Θ range for data collection/°	4.214 to 55.142	4.368 to 53.394
Index ranges	-19 ≤ h ≤ 19, -22 ≤ k ≤ 21, -26 ≤ l ≤ 26	-17 ≤ h ≤ 17, -31 ≤ k ≤ 31, -18 ≤ l ≤ 17
Reflections collected	97733	50743
Independent reflections	22964 [R_{int} = 0.0393, R_{sigma} = 0.0366]	10128 [R_{int} = 0.0914, R_{sigma} = 0.0656]
Data/restraints/parameters	22964/24/1092	10128/32/541
Goodness-of-fit on F^2	1.050	1.064
Final R indexes [I>=2σ (I)]	R_1 = 0.0283, wR_2 = 0.0717	R_1 = 0.0673, wR_2 = 0.1839
Final R indexes [all data]	R_1 = 0.0319, wR_2 = 0.0746	R_1 = 0.0970, wR_2 = 0.2116
Largest diff. peak/hole / e Å^{-3}	1.92/-1.04	2.87/-1.27
CCDC	2277122	2277123

Identification code	**3**	**4**
Empirical formula	$C_{68}H_{112}FeLa_6O_{40}$	$C_{82}H_{126}Fe_2NNd_9O_{55}$
Formula weight	2458.88	3415.69
Temperature/K	298.00	120.00
Crystal system	monoclinic	triclinic
Space group	$P2_1/n$	P-1
a/Å	14.067(6)	15.7445(8)
b/Å	25.297(11)	17.3494(9)
c/Å	14.968(7)	24.9567(12)
α/°	90	95.246(3)
β/°	111.757(13)	98.520(3)
γ/°	90	107.176(3)
Volume/Å^3	4947(4)	6374.9(6)
Z	2	2
ρ_{calc}g/cm^3	1.651	1.767
μ/mm^{-1}	2.751	29.850
F(000)	2416.0	3280.0
Crystal size/mm^3	0.1 × 0.09 × 0.08	0.11 × 0.1 × 0.08
Radiation	MoKα (λ = 0.71073)	CuKα (λ = 1.54178)
2Θ range for data collection/°	4.354 to 50.054	5.386 to 136.926
Index ranges	-16 ≤ h ≤ 14, -29 ≤ k ≤ 30, -17 ≤ l ≤ 17	-18 ≤ h ≤ 18, -20 ≤ k ≤ 20, -30 ≤ l ≤ 28
Reflections collected	26718	64942
Independent reflections	8571 [R_{int} = 0.0953, R_{sigma} = 0.0972]	23216 [R_{int} = 0.1113, R_{sigma} = 0.1227]
Data/restraints/parameters	8571/13/542	23216/58/1365
Goodness-of-fit on F^2	1.049	0.962
Final R indexes [I>=2σ (I)]	R_1 = 0.0736, wR_2 = 0.1877	R_1 = 0.0753, wR_2 = 0.1910
Final R indexes [all data]	R_1 = 0.1165, wR_2 = 0.2211	R_1 = 0.1315, wR_2 = 0.2268
Largest diff. peak/hole / e Å^{-3}	1.97/-1.28	2.71/-2.71
CCDC	2277124	2277059

Reference

[1] G. M. Sheldrick, *Acta Cryst.*, **2015**, *71*. 3.